EXPERIMENTAL AND NUMERICAL INVESTIGATION OF COUNTER-CURRENT STRATIFIED FLOWS IN HORIZONTAL CHANNELS

Thomas Wintterle, Eckart Laurien
University of Stuttgart, Institute for Nuclear Technology and Energy Systems (IKE)
Pfaffenwaldring 31, D-70569 Stuttgart, Germany
Thomas.wintterle@ike.uni-stuttgart.de

Thomas Stäbler, Leonhard Meyer, Thomas Schulenberg
Forschungszentrum Karlsruhe, Institut für Kern- und Energietechnik
Postfach 3640, 76021 Karlsruhe, Germany
Thomas.staebler@iket.fzk.de

Abstract

Counter-current flow regimes of air and water are investigated in the WENKA test facility at Forschungszentrum Karlsruhe. With the fluorescent PIV measurement technique, velocity and velocity fluctuations are measured up to the free surface. A statistical model is presented to correlate the measured void fraction with the turbulent kinetic energy calculated of the measured velocity fluctuations. The experimental data are used to develop a phase interaction model to simulate stratified flows. Two different approaches are compared for turbulence modelling, namely the Prandtl Mixing Length Scale and an extended k-ω model for the two phase region.

Introduction

In the field of safety analysis of nuclear reactors, counter-current stratified flows of water and steam are of great importance. Such thermohydraulic flow phenomena will occur during a Loss of Coolant Accident (LOCA), e.g. a rupture of the main cooling pipe. In such a case, coolant can be injected through the hot leg to prevent the core from overheating. Different flow regimes can occur depending upon the steam leaking from the core. If the steam mass flow is too high, partially reversed flow will occur in the hot leg reducing the volumetric efficiency (ratio of coolant which effectively reaches the core to injected coolant). The objective of the present research is to predict the volumetric efficiency with CFD-methods. Therefore, appropriate models have to be included into the numerical codes. One of the first experiments in horizontal ducts was conducted by Wallis [1], who investigated the stability of counter-current two-phase flows. Most of the investigations in the last decades dealt with the reflux condensation mode during a LOCA ([2], [3], [4], [5]). Few investigations were carried out concerning flow phenomena during hot leg injection. Daly and Harlow [6] conducted a numerical study and derived a model to predict flow reversal during hot leg injection, but no experimental data supported their calculations. Full scale experiments were carried out in the Upper Plenum Test Facilty (UPTF) [7]. The tests covered several injection modes and the results for hot leg injection yielded that the liquid flow was partially reversed for high steam flow rates. Most of the investigations in the last decades, however, presented one-dimensional data and yielded one-dimensional correlations. Kolev [8] demonstrated the need for local experimental data in order to predict such flow phenomena with numerical codes. To provide the required experimental data, the WENKA test facility was built at Forschungszentrum Karlsruhe. This test facility is capable to investigate the flow phenomena of such horizontal counter-current flows under various experimental conditions (Gargallo et. al. [9]).

Test Facility

The test section (Figure 1) has a rectangular cross section (90x110mm) and a length of 470mm. Air and water are used as test fluids and flow counter-currently at ambient temperature and atmospheric pressure. Water circulates in a closed water loop between the water storage tank (600 litres) and the test section. It enters the test section beneath an inlet plate. The inlet plate can be adjusted manually to provide liquid injection heights between 2 and 22mm. A fully developed air flow is fed into the test section via an air inlet channel. It enters the test section above an air inlet plate which is adjusted manually to the height of the liquid inlet plate. After the test section the air is released to the atmosphere again. Several flow regimes can be observed in the test channel depending on the air and water flow rates: Stable stratified flow, including sub- and supercritical flow and the occurrence of a hydraulic jump. After flooding, a reversed flow can be observed where only a reduced amount or even no coolant will be delivered to the end of the test section. In case of reversed flows, the two phases are separated again in a cyclone which is positioned behind the test section. The different possible flow regimes are also shown in Figure 1.

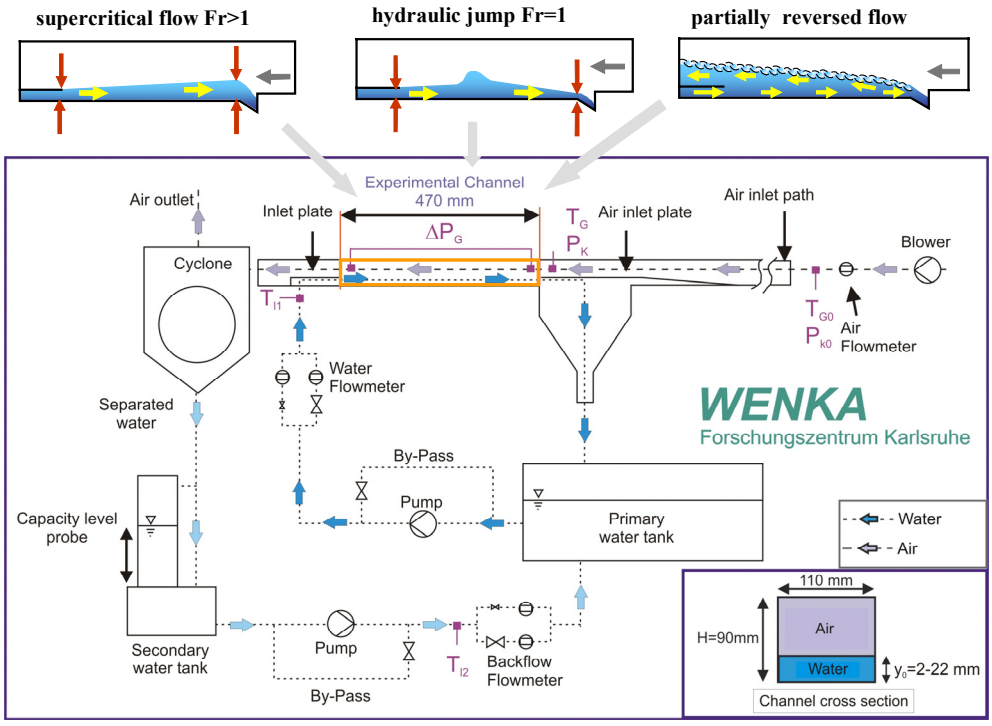

Figure 1: Test facility

Experimental Procedures

The kinematic and turbulent structures of the liquid flow were obtained with Particle Image Velocimetry (PIV). This laser-optical measurement technique delivers the flow quantities without disturbing the flow. The flow is seeded with small particles which follow the flow. These particles are illuminated twice within a short period of time. The particle displacement is calculated by cross-correlation methods. As the time period between the two illuminations is known, the two-dimensional velocity distribution of the flow field can be obtained. A great challenge is to measure the local structures at the moving free surface. The laser light sheet used to illuminate the flow will be reflected at the wavy surface. This prevents the determination of the flow quantities at the free surface and can cause the destruction of the PIV-camera if the laser light is directly reflected onto the camera's CCD-chip. This problem has been solved with a more sophisticated PIV-setup. An optical band-pass filter which is impermeable for the frequencies of the laser light has been positioned in front of the camera lens. Consequently, the reflections at the free surface have been eliminated. In order to record the particle displacement, fluorescent particles have been used. The signal of these fluorescent particles is frequency-shifted compared to the laser light and therefore these frequencies pass the optical filter. The time-averaged velocities of the flow were calculated by:

$$\bar{u} = \frac{1}{\Delta t_{ges}} \int_{t}^{t+\Delta t_{ges}} u(\vartheta)\, d\vartheta \approx \frac{1}{N-1} \sum_{i=1}^{N} u_i \tag{1}$$

where *N* was the number of images taken. The turbulent velocity fluctuations were calculated as:

$$u_{RMS} = \sqrt{u'^2} = \sqrt{\frac{1}{N-1} \sum_{i=1}^{N} (u_i - \bar{u})^2} \tag{2}$$

In order to measure local void fractions, a measurement system including a single tip resistivity probe has been developed. The probe reaches into the test channel through the upper channel wall and can be traversed in vertical direction in steps of 0.005mm. The wavy interfaces of the investigated flows consist of two continuous phases with almost no droplets. Therefore, the second electrode needed for the electrical circuit is represented by the metallic parts of the grounded test facility, which are in constant contact with the liquid phase. The system determines whether the liquid or gaseous phase is in contact with the probe tip. To obtain time-averaged void fractions, the accumulated times for which the probe tip has been in contact with the gaseous phase are divided by the total data acquisition time:

$$\alpha = \bar{\varepsilon} = \frac{1}{\Delta t} \int_{t}^{t+\Delta t} \varepsilon(\vartheta)\, d\vartheta \approx \sum_{i=1}^{N} t_{air,i} \Big/ \Delta t_{measurement} \tag{3}$$

with a total data acquisition time of 120s and an acquisition rate of 200Hz.

Experimental Results

This chapter presents the experimental results for different investigated supercritical flows. The measurements were conducted in the middle plane of the test section at two different positions *x* along the channel for two different water inlet heights y_0. The experimental conditions are given in Table 1. Each experimental run was conducted independently. Therefore, also the Reynolds-numbers of the runs within each case differ to some extent.

case	run	y_0 [mm]	x [mm]	Q_L [l/min]	Q_G [l/min]	Fr_{LO} [-]	Re_L [-]	Re_G [-]
(I)	(a)	9	235	41,7	59,1	2,36	6520	37372
	(b)	9	380	41,7	59,1	2,35	6615	37541
(II)	(c)	15	235	71,4	59,3	1,88	11211	39171
	(d)	15	380	71,3	59,7	1,88	11397	39077

Table 1: Experimental conditions

The inlet Froude-number is given by the ratio of inertial forces to gravitational forces and can be written as:

$$Fr_{L0} = u_0 / \sqrt{(g \cdot y_0)} \tag{4}$$

where u_0 denotes the mean velocity at the liquid injection, which is given by the liquid flow rate. The liquid Reynolds-number has also been calculated with the liquid mean velocity and with the inlet liquid height. The characteristic length for the Reynolds number for the air is given by the hydraulic diameter d_h:

$$d_h = 4A/U = 4(h - y_0)\, z / 2[(h - y_0) + z] \tag{5}$$

whereas the height of the air inlet plate above which the air enters the test section has been adjusted to the liquid inlet height y_0. Furthermore, h denotes the channel height and z the channel depth.

Figure 2 shows the time-averaged velocity profiles for the presented flows. The wall normal coordinate y is plotted against the local time-averaged liquid velocity components u in horizontal direction and v in vertical direction normal to the bottom wall, respectively.

In all cases, the influence of the bottom wall can be seen in the velocity profiles in horizontal direction where the liquid flow is slowed down near the wall. In the upper part of the liquid flow near the maximum liquid heights, the liquid phase is slowed down by the counter-current flow of air. The maximum velocities in horizontal direction can be found just below the maximum liquid heights. The magnitudes of the maximum vertical velocities reach from 1.5 to 4.5 % of the mean velocities in horizontal direction. The liquid heights of supercritical flows increase in direction of the flow, which can also be seen in the positive values of the mean vertical velocities. As explained above it is obvious that the vertical velocities are damped by the bottom wall as well as by the gas-liquid interface.

The velocity fluctuations can be seen in Figure 3. The magnitudes of the horizontal velocity fluctuations u_{rms} are always higher than the vertical fluctuations v_{rms}. It can clearly be seen, that the fluctuations increase remarkably in the upper part of the flow. The increase of the horizontal fluctuations can be explained by the deceleration of the flow. The increase of the vertical fluctuations is due to the vertical motion of the interfacial waves.

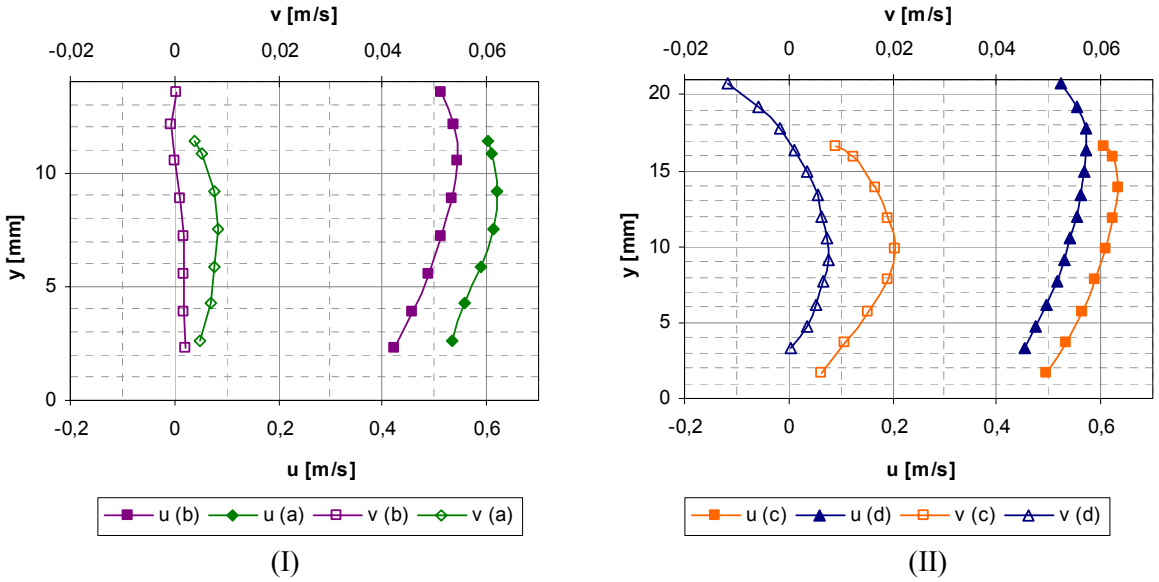

Figure 2: Velocity profiles: (I) y_0=9 mm, (II) y_0=15 mm

Figure 4 shows the measured void distributions. Principally, a stratified liquid-gas flow can be divided into three different sections. The lower part of the flow is represented by a closed liquid film without gas (α=0). In contrast to that, only gas is present in the upper part of the flow (α=1). The phase interaction section between the lower and upper section is characterized by a wavy interface (0< α <1). The void profiles show a linear behaviour in the bulk area of the phase interaction section. The gradient of the void distributions increases heavily towards the single phase conditions α =0 and α =1.

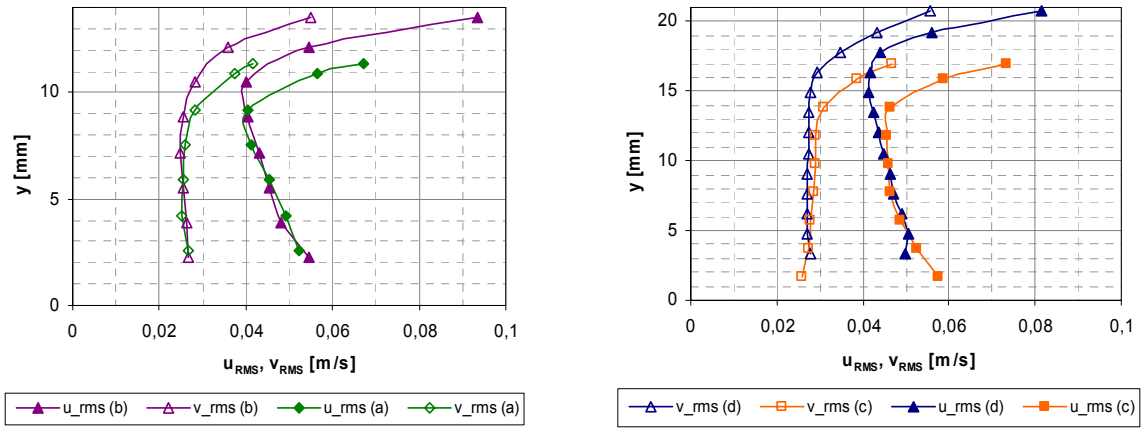

(I) (II)

Figure 3: Rms-velocity profiles: (I) y_0=9 mm, (II) y_0=15 mm

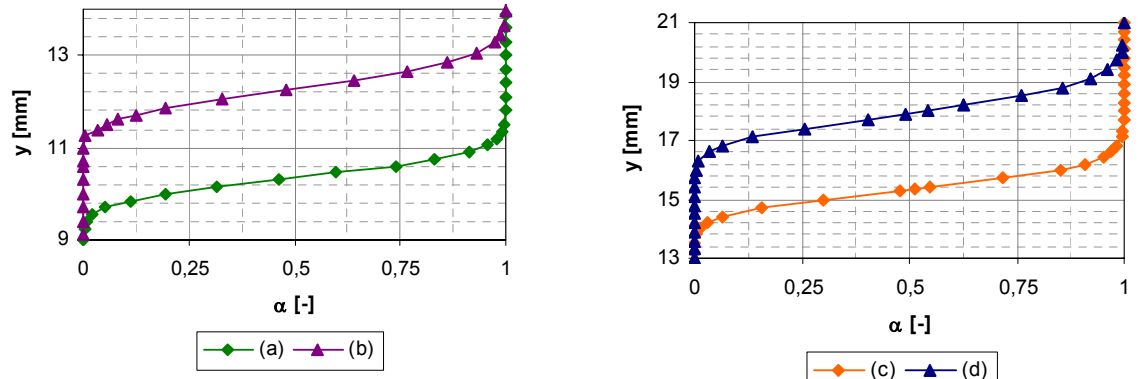

(I) (II)

Figure 4: Void distribution profiles: (I) y_0=9 mm, (II) y_0=15 mm

Statistical Model

A statistical model for the interaction of fluid particles can describe the measured void profiles. The velocity measurements yield a Gaussian distribution of the local velocities which has a probability *P(v)* as:

$$P(v) = \frac{1}{\sqrt{2\pi\overline{v'^2}}} \exp\left(\frac{(v-\bar{v})^2}{2\overline{v'^2}}\right) \tag{6}$$

The exponent in Eq. (6) can be rewritten as an energy ratio when extended by $\rho_L/2$ and if generalized to three dimensions:

$$P(E_{kin}) = \frac{1}{\sqrt{2\pi\rho_L \bar{k}_L}} \exp\left(-\frac{E_{kin}}{2\rho_L \bar{k}_L}\right), \tag{7}$$

where E_{kin} is the turbulent kinetic energy of a fluid particle and $\bar{k}_L$ is the local time-averaged turbulent kinetic energy within the liquid. Let us regard the interaction of two fluid particles: If the kinetic energy of the first particle is high enough to elevate the second particle from a position *y* to a higher position *y+dy*, Eq. (7) yields the probability of the potential energy of the second particle:

$$P(\Delta E_{pot}) = \frac{1}{\sqrt{2\pi\rho_L \bar{k}_L}} \exp\left(-\frac{\Delta\rho g\, dy}{2\rho_L \bar{k}_L}\right), \tag{8}$$

with $\Delta E_{pot} = \Delta\rho g\, dy$ as the increase of potential energy of the second particle. The probability that a first particle transfers its kinetic energy to the potential energy of the second particle is:

$$P_1 = (1-\alpha(y))\alpha(y+dy)P(\Delta E_{pot}), \tag{9}$$

because liquid must be at elevation y, for which case we have the probability (1-α(*y*)) and an empty space must be at elevation *y*+*dy*, which has the probability α(*y*+*dy*). Inserting Eq. (8) into Eq. (9) yields:

$$P_1 = (1-\alpha(y))\alpha(y+dy)\frac{1}{\sqrt{2\pi\rho_L \bar{k}_L(y)}}\left(1-\frac{\Delta\rho g\, dy}{2\rho_L \bar{k}_L(y)}\right) \tag{10}$$

The probability for the reverse process, where a fluid particle at position *y*+*dy* transfers its potential energy to a particle at position *y* can be written as:

$$P_2 = \alpha(y)(1-\alpha(y+dy))\frac{1}{\sqrt{2\pi\rho_L \bar{k}_L(y)}} \tag{11}$$

Under equilibrium conditions, the probabilities P_1 and P_2 must be equal. Equating both probabilities and dissolving the equation yields:

$$\frac{d\alpha}{dy} = \frac{\Delta\rho g}{2\rho_L \bar{k}_L(y)}(1-\alpha(y))\alpha(y). \tag{12}$$

Eq. (12) represents a differential equation which relates the local void fraction to the local turbulent quantities of the flow. The turbulent kinetic energy of a flow is always three-dimensional and can be expressed as:

$$\bar{k}_L = \frac{1}{2}(\overline{u'^2} + \overline{v'^2} + \overline{w'^2}) \tag{13}$$

As PIV represents a two-dimensional measurement technique an assumption of the third component $\overline{w'^2}$ has to be made. Here $\overline{w'^2}$ was assumed to be the same as $\overline{v'^2}$. A comparison of this statistical model with experiments can be found in Stäbler et. al. [10].

Numerical part

Surface waves can only be simulated with very fine resolved grids or DNS calculations. For real geometries a statistical time-averaged modelling has to be used for such surface waves. The incompressible Two-Fluid Equations (see Drew and Passman [11]) describe a set of coupled Navier-Stokes Equations which can exchange mass, momentum and energy between the two phases. For stratified flows in a counter-current mode of air and water only small surface waves will occur. At the

free surface only momentum is transferred from the water to the air and vice versa. The physical momentum exchange is modelled with a phase exchange model.

The statistical time-averaging of the surface waves smears the free surface in between the amplitude of the surface waves. Numerically this can be treated as a dispersion force F_s acting normal to the free surface and which is proportional to the gradient of the void fraction.

$$F_s = C \cdot \nabla \alpha_G \tag{14}$$

For horizontal flows the dispersion force is balanced with the buoyancy force which can be written for two phase flows with the unit of force per volume,

$$F_A = (\rho_L - \rho_G) \cdot g \cdot \alpha_L \cdot \alpha_G \tag{15}$$

yielding the following differential equation:

$$\frac{d\alpha_G}{dy} = \frac{\Delta\rho \cdot g}{C} \cdot \alpha_G \cdot (1 - \alpha_G) \tag{16}$$

Comparing the approach of the phase exchange model (Eq. (16)) with the derived theory of the experimental data (Eq. (12)) leads to the proportionality factor of the dispersion force.

$$C = 2 \cdot \rho_L \cdot k_L \tag{17}$$

The proportionality factor of the dispersion force depends on the turbulent kinetic energy, which could be expected because with increasing gas velocity the wave amplitudes are increasing and also the turbulent kinetic energy. Comparing the experimental data and the numerical model leads to the dominant forces which are the buoyancy force and the dispersion force caused by the turbulence. The surface tension force plays no significant role for the case of horizontal flows and can be neglected which is also confirmed by calculating the Weber number.

The drag exerted due to the shear stress at the interface is modelled by the drag force implemented in CFX-10,

$$F_D = C_D \frac{\rho^*}{2} \frac{\alpha_L \cdot \alpha_G}{d_{char}} \cdot u_{rel}^2 \tag{18}$$

where C_D is the drag coefficient, ρ^* the mixture density, $\alpha_L \alpha_G / d_{char}$ the interfacial area density and u_{rel} the slip velocity. C_D and d_{char} have to be modelled for the phase interaction model. To find a geometrical interpretation for the characteristic length scale for turbulent and wavy surfaces is not possible like for bubbly flow. Instead a derivation is presented to correlate the characteristic length scale with the shear stress at the interface.

$$\tau_i = \lambda_i \frac{\rho_G}{2} \cdot u_{rel}^2 \tag{19}$$

The drag force is integrated over the volume of the smeared surface and is equated with the integrated shear stress over the free surface, which yields the following correlation.

$$\int_{y_{min}}^{y_{max}} C_D \frac{\rho^*}{2} \frac{\alpha_L(y) \cdot \alpha_G(y)}{d_{char}} \cdot u_{rel}^2 \cdot dy = \lambda_i \frac{\rho_G}{2} \cdot u_{rel}^2 \tag{20}$$

E.g. from Wang and Mayinger [12] the interfacial friction factor for turbulent flows is known. This integral can be solved by substituting dy by the differential equation (16) which correlates the drag coefficient with the characteristic length scale.

$$\frac{C_D}{d_{char}} = \frac{\lambda_i \cdot \rho_G \cdot (\rho_L - \rho_G) \cdot g}{C \cdot \rho^*} \tag{21}$$

The ratio between the drag coefficient and the characteristic length scale reduces the number of coefficient which has to be calibrated. In the simulation a value of d_{char}=0.003m is set for the characteristic length scale and C_D=0.1 is an appropriate value for the momentum exchange at the free surface calibrated with the experimental data for supercritical flow.

Turbulence modelling is also important for an accurate prediction of the velocity profiles both in the phase interaction region and the near wall region. The velocity of the gas phase feels the fluid phase as a moving wall and vice versa. In this free surface region the velocity profiles for both phases behave approximately as boundary layers and have to be accounted for by the turbulence modelling. In order to gain a better understanding of the turbulence phenomena a Prandtl mixing length is used. The eddy viscosity calculates to:

$$\mu_t = \rho \cdot l^2 \left| \frac{\partial u}{\partial y} \right| \tag{22}$$

Using the non-dimensional universal wall function and differentiate with respect to y and using the assumption for the shear stress yielding the following mixing length correlation for the near wall after Prandtl:

$$l = \kappa \cdot y \tag{23}$$

Comparing the experimental data with the logarithmic wall function in figure 6 a deflection for the experimental data can be observed. This region is known as defect layer and is caused by the free turbulence in the outer area of the boundary layer. (See Rotta [13]). Coles [14], for example, proposed to extend the wall function with a so called wake function to model the defect layer. But for the supercritical flow the defect layer for the liquid phase shifts to lower y^+. In this case the wake function of Coles fails to predict the behaviour for the supercritical flow conditions. Instead we have developed an empirical correlation which takes account of the geometry and the flow conditions in the test facility.

$$u^+ = \frac{1}{\kappa} \ln(y^+) + C^* + \frac{A}{\kappa} \left[1 - \frac{1}{1 + e^{\left(\frac{y^+ - 60}{30} \right)}} \right] \tag{24}$$

Applying the same procedure as described above for the derivation of the mixing length for the near wall flow the following mixing length correlation can be derived for the wake function.

$$l = \kappa \cdot y \frac{1}{1 - \frac{e^{\left(\frac{y^+ - 60}{30} \right)}}{(1 + e^{\left(\frac{y^+ - 60}{30} \right)})^2} \cdot A \cdot y^+} \tag{25}$$

A is a constant to adjust the amplitude of the defect layer and is set to 1.5. For numerical purposes the function is limited to a maximum $l_{\max} = 0.2 \cdot h_{inlet}$ to avoid numerical instabilities and unphysical overprediction of the eddy viscosity. To take account of the turbulence at the free surface a modified mixing length is used in the two phase layer which takes the value of $l_{surface} = 0.00025$. The inner layer is modelled with $l = h_{inlet} \cdot 0.125$. For the case of supercritical flow the mixing length in the two phase region is smaller compared with the inner layer. This effect can be explained with the turbulence damping at the free surface. Figure 5 illustrates the different layers and mixing length scales.

The results using the Prandtl mixing length model are sketched in the figures 7 and 8. The boundary conditions are listed in table 1. As apparent from table 1 only supercritical flow is considered. The proposed wake function resolves the eddy viscosity very accurately in the near wall region for all cases. The prediction of the inner layer fails to predict the amount of the eddy viscosity because the velocity gradient reaches zero.

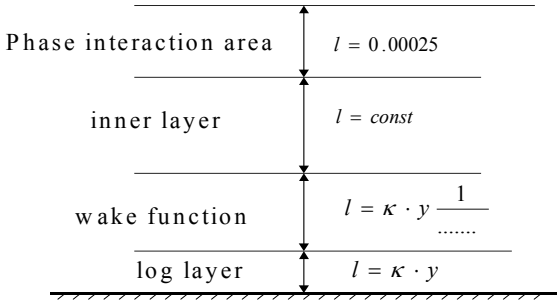

Figure 5: Mixing length scales over the liquid film height

Due to this fact the eddy viscosity goes to zero, too. This is a well know phenomenon and can be explained with the missing of turbulence transport. Prandtl considered the production and dissipation of turbulence as a constant process but in many flow patterns the amount of turbulence depends on the flow history. This means that transport and diffusion of turbulence plays an important role, too. Also equation (17) indicates, that the turbulent kinetic energy is important for the phase interaction process.

To overcome the deficiency of the Prandtl mixing length a two-equation turbulence model is used. Here the k-ω model of Wilcox [15] is chosen instead the k-ε model because the defect layer is resolved better by the k-ω model. To take account of the turbulence damping in the phase interaction region the k-ω model is extended by an additional production term in the ω-equation. This term leads to a damping of the turbulent kinetic energy in the k-equation. Lopez de Bertodano et. al. [16] derived a Reynolds Stress Model for a two-fluid model. He proposed to use an additional production and diffusion term for the k-equation and a production term for the dissipation equation ε. In the case of countercurrent flow only turbulence damping plays a role and is accounted for by the ω-equations like the dissipation equation of Lopez de Bertodano. The k- and extended ω-equation calculates to:

$$\frac{\partial(\rho k)}{\partial t} + \frac{\partial(\rho u_j k)}{\partial x_j} = P_k + \frac{\partial}{\partial x_j}\left(\mu + \frac{\mu_t}{\sigma_k}\frac{\partial k}{\partial x_j}\right) - \beta' \rho k \omega \tag{26}$$

$$\frac{\partial(\rho \omega)}{\partial t} + \frac{\partial(\rho u_j \omega)}{\partial x_j} = a\frac{\omega}{k}P_k + \frac{\partial}{\partial x_j}\left(\mu + \frac{\mu_t}{\sigma_w}\frac{\partial \omega}{\partial x_j}\right) - \beta \rho \omega^2 + a^{2\varphi}\frac{\omega}{k}P_k^{2\varphi}\alpha_1\alpha_G \tag{27}$$

a	$a^{2\phi}$	β'	β	σ_k	σ_ω
5/9	0.0006 (15mm) 0.0009 (9mm)	0.09	0.075	2	2

Table 2: k-ω model constants

The calculations are performed with the finite volume code CFX-10 with FORTRAN routines for the dispersion force. The transient computational mode is used. The figures 9 and 10 show the velocity profiles for the case (c) and (d) with a parameter study for a constant $a^{2\phi}$. If $a^{2\phi}$<0.0025 the momentum exchange due to the amount of calculated turbulence is too high and the hydraulic jump is initiated. Partially reversed flow occurs only for the original k-ω model which can be determined from the negative value for the flow velocity ($u^* = u/\overline{u}_m$ and $y^* = y/h \max(\alpha_l = 0)$ is the axis notation). The curve for the original k-ω model is sketched in figure 13. The figures 11 and 12 show the influence of the constant $a^{2\phi}$ for the turbulence production at the interface. The turbulence level of the experiments is increasing at the interface whereas Tu is defined by $Tu = \sqrt{u'^2+v'^2+w'^2}/\overline{u}_m$. For the turbulence only a part of the parameter study is shown due to the strong increasing of the turbulence level for less damping at the interface. In the near wall region a divergence of the turbulence intensity of about a factor 1.5 can be seen, but the eddy viscosity is calculated with the right amount of intensity which is obvious from the velocity profiles. As apparent of the parameter study for the constant $a^{2\phi}$ the turbulence level is calculated best by a value of $a^{2\phi}$=0.0006.

Conclusions

Supercritical flows under counter-current flow conditions are investigated experimentally in the WENKA test facility with the Fluorescence Particle Image Velocimetry and a single tip resistivity probe. Experimental data are available up to the free surface. Time-averaged local velocity fields, time-averaged local velocity fluctuations and void fraction distributions are presented and discussed. The velocities in wall normal direction show very low values compared to the streamwise velocities. Near the free surface, the liquid is decelerated by the counter-current flow of air. The velocity fluctuations in vertical and horizontal direction increase remarkably within the wavy two-phase region. A statistical approach is presented which correlates the turbulent kinetic energy of the liquid phase with the void fraction distribution. This approach testifies a major influence of the turbulent and potential energy of the liquid phase on the two-phase region. The derived differential equation is implemented into the numerical code CFX-10 to model the momentum transfer for the two phase region. The behaviour of the turbulence is first modelled with the mixing length and subsequently with an extended k-ω model with an additional term, which takes into account the turbulence effects in the two phase layer. The horizontal mean streamwise velocity component indicates a defect layer for the liquid phase near the wall. For the mixing length a wake function is derived to model the defect layer and good results are achieved for the near wall flow. The mixing length fails to predict the correct amount of eddy viscosity in the inner layer due to transport phenomena of turbulence. Therefore, the two-equation k- ω turbulence model is used. A parameter study is performed for the k- ω model which indicates a best practice value for the additional two phase turbulence term. Applying this best practice value yields numerical predictions which are in good conformity with the experimental results.

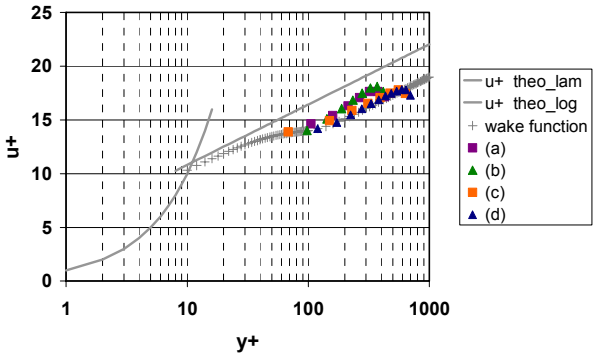

Figure 6: Wake function

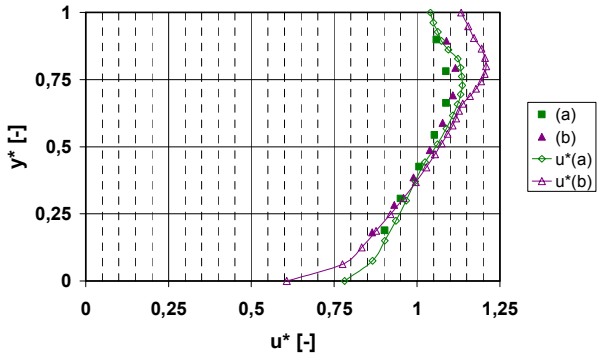

Figure 7: Velocity profile case (a) and (b) Prandtl

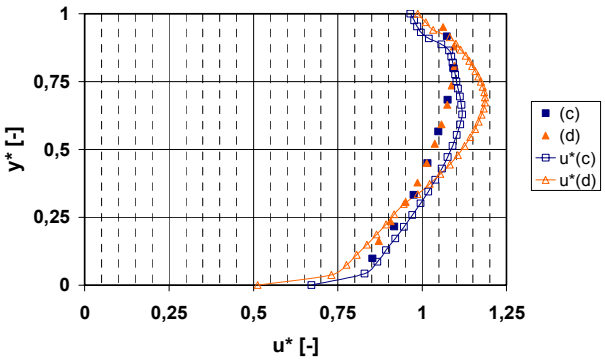

Figure 8: Velocity profile case (c) and (d) Prandtl

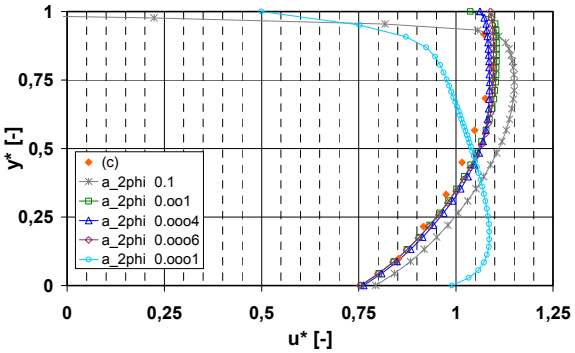

Figure 9: Parameter study velocity profile case (c)

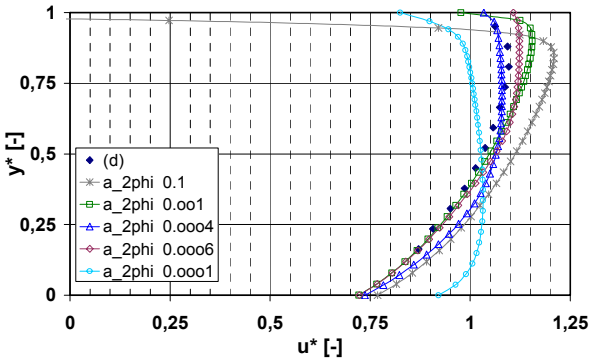

Figure 10: Parameter study velocity profile case (d)

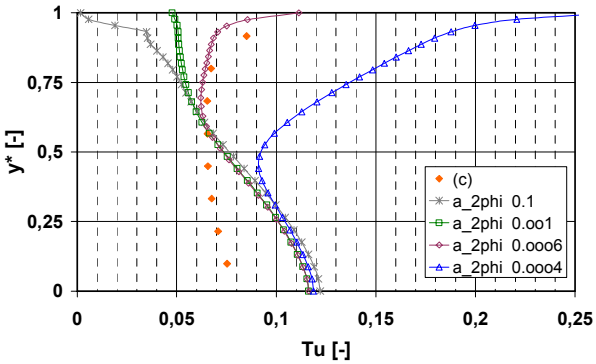

Figure 11: Parameter study turbulence level case (c)

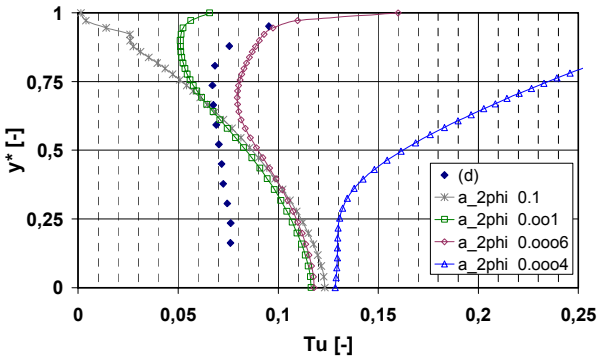

Figure 12: Parameter study turbulence level case (d)

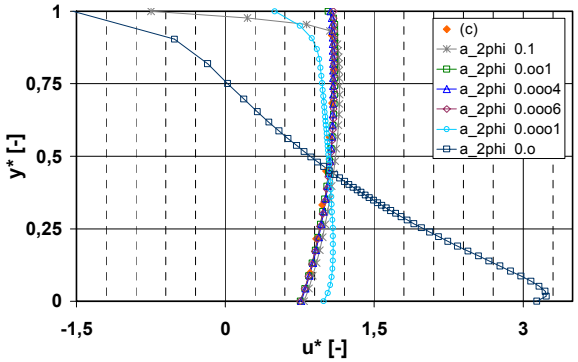

Figure 13: Case (c) with original k-ω model

Literature

[1] Wallis, G.B., One-dimensional Two-Phase Flow, McGraw-Hill Book Company, London, 1969

[2] Ohnuki, A., Adachi, H. and Murao, Y., Scale Effects on Countercurrent Gas-Liquid Flow in a Horizontal Tube Connected to an Inclined Riser, Nuclear Engineering and Design, Vol. 107, 1988, pp. 283-29

[3] Richter, H.J., Wallis, G.B., Carter, K.H. and Murphy, S.L., Deentrainment and Countercurrent Air-water Flow in a Model PWR Hot Leg, NRC-0193-9, U. S. Nuclear Regulatory Commission, Washington D. C., 1978.

[4] Siddiqui, H., Banerjee, S. and Ardron, K.H., Flooding in an Elbow between a Vertical and a Horizontal or Near-horizontal Pipe. Part I: Experiments, Int. J. Multiphase Flow, vol. 12, No. 4,1986, pp. 531-541

[5] Lopez de Bertodano, M.L., Countercurrent Gas-Liquid Flow in a Pressurized Water Reactor Hot Leg, Nuclear Science and Engineering, vol. 117, 1994, pp. 126-133.

[6] Daly, B.J. and Harlow, F.H., A Model of Counter-current Steam-Water Flow in Large Horizontal Pipes, Nuclear Science and Engineering, Vol. 77, 1981, pp. 273-284.

[7] Damerell, P.S., Simmons, J.W., Reactor Safety Issues Resolved by the 2D/3D Program, Prepared jointly by Japan Atomic Energy Research Institute, Gesellschaft für Anlagen- und Reaktorsicherheit (GRS) mbH, Siemens AG, UB KWU, U.S. Nuclear Regulatory Commission, Los Alamos National Laboratoy, MPR Associates, Inc., 1993

[8] Kolev, N.I., Seitz, H. and Roloff-Bock, I., Hot-Leg Injection: 3D versus 1D Three Velocity Fields Mode-ling and Comparison with UPTF Experiment, Proc. of the ExHFT-5, 5th World Conference on Experimental Heat Transfer, Fluid Mechanics and Thermodynamics, Thessaloniki, Greece, 2001.

[9] Gargallo, M., Schulenberg, T., Mayer, L., Laurien, L., Counter-Current Flow Limitations during Hot Leg Injection in Pressurized Water Reactors, Nuclear Engineering and Design, Vol. 235, 2005, pp. 785-804

[10] Stäbler, T.D., Meyer, L., Schulenberg, T., Laurien, E., Turbulence and Void Distribution in Horizontal Counter-current Stratified Flow, Proc. 17th Int. Symposium on Transport Phenomena, Toyama, Japan, 2006

[11] Drew, D.A., Passman, S.L., Theory of Multicomponent Fluids, Springer, New York, 1999

[12] Wang, M.J., Mayinger, F., Simulation and analysis of thermal-hydraulic phenomena in a PWR hot leg related to SBLOCA, Nuclear Engineering and Design, Vol. 155, 1995, pp. 643-652

[13] Rotta, J.C., Turbulente Strömungen, Teubner Verlag, Stuttgart, 1972

[14] Jischa, M., Konvektiver Impuls-, Wärme- und Stoffaustausch, Vieweg&Sohn, Braunschweig/Wiesbaden, 1982

[15] Wilocx, D.C., Turbulence Modeling for CFD, DCW Industries, 1998

[16] Lopez de Bertodano, M.L., Lee, S.J., Lahey, R.T., Drew, D.A., The Prediction of Two-Phase Turbulence and Phase Distribution Phenomena Using a Reynolds Stress Model, J. of Fluids Engineering, Vol. 112, 1990, pp. 107-113